

Research Article

Weighted LabPQR Interim Connection Space Based on Human Color Vision for Spectral Color Reproduction

Guangyuan Wu,¹ Zhen Liu,² Shengwei Yang,³ Ming Zhu,⁴ and Pan Liu²

¹ School of Optical-Electrical and Computer Engineering, University of Shanghai for Science and Technology, Shanghai 200093, China

² College of Communication and Art Design, University of Shanghai for Science and Technology, Shanghai 200093, China

³ Department of Printing and Packaging Engineering, Shanghai Publishing and Printing College, Shanghai 200093, China

⁴ Department of Materials and Chemical Engineering, Henan Institute of Engineering, Zhengzhou 450007, China

Correspondence should be addressed to Zhen Liu; lunaprint@163.com

Received 14 July 2014; Accepted 10 October 2014; Published 27 October 2014

Academic Editor: Shinichi Morita

Copyright © 2014 Guangyuan Wu et al. This is an open access article distributed under the Creative Commons Attribution License, which permits unrestricted use, distribution, and reproduction in any medium, provided the original work is properly cited.

A weighted LabPQR interim connection space, based on human color vision, is proposed for retaining more visual color information. A new weight function proposed in our paper is connected with color-matching function and then further weighted the PQR dimensions of LabPQR compared with the other two weight functions and nonweight function. The results indicated that weighting obviously improved the colorimetric representing accuracy and robustness compared with nonweighting, and the new weight function outperformed the other two weight functions. The weighted LabPQR of the new weight function is most suitable for spectral color reproduction.

1. Introduction

The spectral reflectance is defined as an object “fingerprinting” that accurately carries the fundamental color information, so spectral color reproduction could match originals under arbitrary illuminants and observers [1–3]. However, a high-dimensional spectral data need large storage space and computational complexity. In addition, the raw spectral data is not suited for spectral image processing, gamut boundary description, and spectral gamut mapping in the spectral color reproduction in many applications such as textile color, art reproduction, and printers with inks [3–6]. So it is necessary to construct an interim connection space (ICS) both for spectral color representation and reproduction.

In the quest for an optimal spectral color reproduction, an impressive number of ICSs have been proposed in the literature, and ICSs are classified into two types of categories. The first type is the algorithm that applies multivariate statistical analysis theory to optimize spectral color information. Bakke et al. [7] proposed PCA-based ICS, which applied principal component analysis (PCA) on dimensionality reduction of the spectra and spectral reconstruction. Zhang et al. [8] proposed two ICSs called ICS_{.2SI}

and ICS_{.3SI}, which applied PCA on extracting the widely used illuminants and light sources. These ICSs have the higher spectral and colorimetric representing accuracy and no obvious illuminants selective property. However, these ICSs have not effectively gamut boundary, gamut mapping algorithms, and spectral gamut visualization. In addition, ICSs are not compatible with the widely used colorimetric management system and have no actual physical meaning.

The second type called compensation approach reinserts metameric black spectrum to compensate for the loss of spectral details caused by the colorimetric tristimulus values. Derhak and Rosen [9] had proposed an ICS called LabPQR with six dimensions. The first three dimensions were CIE L*a*b* values under a specific viewing condition, and the additional dimensions were spectral reconstruction dimensions describing a metameric black (PQR) with PCA. As a matter of fact, the LabPQR ICS could well represent the spectral information with low dimension, and most of the proposed spectral gamuts mapping algorithms in LabPQR were based on the optimal method [8]. Several variations of the LabPQR had been proposed recently, such as the LabRGB color space [10] and XYZLMS color space [3]. These ICSs could be better to be compatible with the widely used colorimetric

management system and spectral gamut visualization. In addition, LabPQR have effectively gamut boundary and gamut mapping algorithms [11]. It had reported that LabPQR could be used successfully in several applications [12, 13]. However, these ICSs have obvious illuminants dependence property. In additional, the LabPQR ICS is with high spectral but low colorimetric representing accuracy. The main reason is that PQR dimensions of LabPQR apply PCA to extract the residual error of the spectral reflectance, and are not weighted by the human color vision that usually has different sensitivities over different wavelengths.

This paper presents a weighted LabPQR ICS based on human color vision for the spectral color reproduction, which is the desire to achieve a visually more spectral color mapping between reproductions and originals. To define the most optimal weight function, three different weight functions were tested. These weighted LabPQR (wLabPQR) ICSs were evaluated under different illuminants and light sources compared with the traditional, nonweighted LabPQR ICS.

2. Mathematical Background

2.1. LabPQR [9, 11–13]. The LabPQR is a six-dimensional ICS. The first three dimensions are CIELAB values under a specific condition, and the additional dimensions are spectral reconstruction dimensions (PQR). The PQR coordinates represent the spectral difference between original and reconstructed spectra from colorimetric values.

Spectral reconstruction from six-dimensional LabPQR could be determined as

$$\hat{\mathbf{R}} = \mathbf{T}\mathbf{N}_c + \mathbf{V}\mathbf{N}_p, \quad (1)$$

where \mathbf{T} is a n by 3-transformation matrix, \mathbf{V} is a n by 3 matrix describing PQR bases, \mathbf{N}_c is a tristimulus vector, \mathbf{N}_p is a vector of PQR values, and n counts wavelength λ . Note that \mathbf{T} is applied to tristimulus values converted from CIELAB values. Using a set of the tristimulus vectors, the transformation matrix \mathbf{T} is determined by a matrix calculation using the least square analysis:

$$\mathbf{T} = \mathbf{R}\mathbf{N}_c^T(\mathbf{N}_c\mathbf{N}_c^T)^{-1}, \quad (2)$$

where \mathbf{R} is measured spectral reflectance of training samples; the superscript “ T ” shows the pseudoinverse of the proposed matrix.

The PQR bases \mathbf{V} are derived from principal component analysis (PCA) on a set of spectral differences between the original spectra and the reconstructed spectra through the inverse transformation with \mathbf{T} from \mathbf{N}_c . This spectral difference is expressed as

$$\mathbf{E} = \mathbf{R} - \mathbf{T}\mathbf{N}_c. \quad (3)$$

Only the first three eigenvectors are preserved as the PQR bases:

$$\mathbf{V} = (\mathbf{v}_1, \mathbf{v}_2, \mathbf{v}_3), \quad (4)$$

$$\hat{\mathbf{E}} = \mathbf{V}\mathbf{N}_p,$$

where \mathbf{v}_i are eigenvectors in a set of the spectral difference.

2.2. Weighted LabPQR (wLabPQR). It is clear that the PCA is the well-known linear model that equally treats spectral reflectance over the whole wavelength, which could not well represent the characteristic of color information [14, 15]. The purpose of wPCA is to improve the color reproduction accuracy at the cost of the accuracy of spectral reconstruction in color technology and science [16, 17].

In the wPCA, it is noted that, before calculating the correlation matrix \mathbf{C}_w , each sample point requires being multiplied or weighted with proper coefficients or a weight function $w(\lambda)$, resulting in weighted data \mathbf{E}_w ,

$$\mathbf{C}_w = \mathbf{E}_w\mathbf{E}_w^+ = \mathbf{W}\mathbf{E}[\mathbf{W}\mathbf{E}]^+, \quad (5)$$

where the matrix \mathbf{W} is a diagonal matrix with main diagonal of the values of the weigh function $w(\lambda)$. The superscript “ $+$ ” is the matrix transpose. After reproduction, this same weight function can be separated from the spectral data to achieve representatives of the original spectral curves [17]. Consider

$$\hat{\mathbf{E}} = \mathbf{V}(\mathbf{W}\mathbf{V})^T\mathbf{W}\mathbf{E}. \quad (6)$$

2.3. Weight Function. The main goal of the wPCA algorithm is to minimize the weighted squared reconstruction error [18]:

$$\mathbf{e} = \sum \mathbf{W}(\mathbf{E} - \hat{\mathbf{E}})^2 = \sum (\sqrt{\mathbf{W}\mathbf{E}} - \sqrt{\mathbf{W}\hat{\mathbf{E}}})^2 \rightarrow \mathbf{Min}. \quad (7)$$

To evaluate the performance of the weight functions, three weight functions were selected. The weight functions are not limited, but the color-matching functions well reflect human vision characteristics. Three weight functions plotted in Figure 1 are connected with CIE1931 $\bar{x}(\lambda)$, $\bar{y}(\lambda)$, and $\bar{z}(\lambda)$ color-matching function that involves brightness information and chromatic information.

The first weight function $w_1(\lambda)$ (WF1) was introduced by Tian and Tang [16], which is generated by adding the three matching functions and normalizing the maximum of value to be 1:

$$w_1(\lambda) = \frac{\bar{x}(\lambda) + \bar{y}(\lambda) + \bar{z}(\lambda)}{2.14631}. \quad (8)$$

The second weight function $w_2(\lambda)$ (WF2) is generated by adding the three matching functions to the constant functions, which normalize the maximum of value to be 1. The WF2 was introduced by Laamanen et al. [17]. Consider

$$w_2(\lambda) = \frac{\bar{x}(\lambda) + \bar{y}(\lambda) + \bar{z}(\lambda) + 1}{3.14631}, \quad (9)$$

because values of CIE1931 $\bar{x}(\lambda)$, $\bar{y}(\lambda)$, and $\bar{z}(\lambda)$ color-matching function are not less than zero. According to (7), we proposed the third weight function $w_3(\lambda)$ (WF3) generated by calculating the square root of adding the three matching functions, which normalize the maximum of value to be 1:

$$w_3(\lambda) = \frac{\sqrt{\bar{x}(\lambda) + \bar{y}(\lambda) + \bar{z}(\lambda)}}{1.46503}. \quad (10)$$

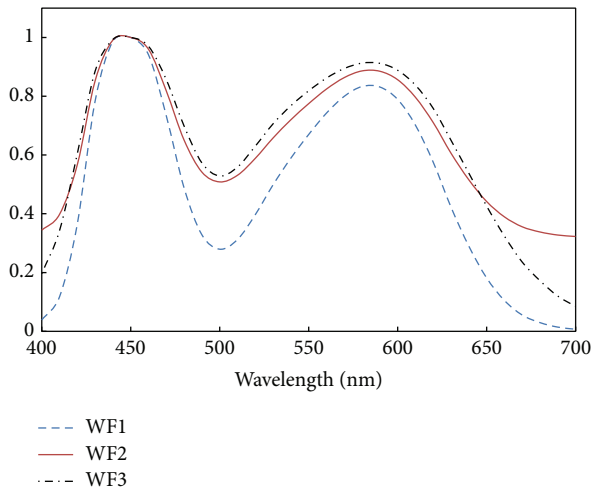


FIGURE 1: The weigh function $w(\lambda)$.

3. Experiments and Procedure

To evaluate the performance of nonweighted LabPQR (ICS_NW) and wLabPQR with three different weight functions (ICS_WF1, ICS_WF2, and ICS_WF3), all the four ICS were constructed, respectively. The CIE1931 2° standard observer was adopted for all four ICSs. The CIE standard illuminant D65 was employed to construct the first three dimensions of the four ICSs.

The spectral reflectance of Munsell (1269 chips) and spectral image (fruits_and_flowers) [19] were adopted to construct and assess the performance of the ICSs. For most applications, these continuous functions could be sampled at 10 nm intervals without a signification loss of accuracy [20]. So, all the spectrums, light sources, and illuminants were sampled at 10 nm intervals between 400 and 700 nm. After that, all the parameters of the four ICSs were determined; the spectrums of the testing samples were converted to the four ICSs and then transformed back to spectral reflectance.

The color difference is a more powerful tool to access the performance of ICS as the eventual criterion for evaluating the spectral color reproduction accuracy is the human color vision under various illuminating environments [8]. Therefore, the CIELAB color differences between the original and reconstructed spectrum of Munsell and spectral image testing samples are calculated under the CIE standard illuminants, light emitting diode (LED) light sources, and tungsten halogen (TH) light source. The dominant spectral power distributions (SPDs) of the selected illuminants and light sources were relatively smooth and with various distributions, which did not contain much spiky radiance. So only the CIE illuminants (A, B, C, D50, D55, and D75), the LED light sources (Sylvania Concord 2048794, Photon Star CS5, Erco Optec Spotlights, Synergy 1003605 S12, Synergy 1003607 NF34, Cooper DL11-WS-WW, GE Par 30, Philips EnduraLED MR16, Erco Light Board V01, MSI iPAR3830021D, Erco ERCO Large Flood, Philips Philips Par38, Solais LR38, and Philips MASTER LEDspot MV), and the TH light sources (Solux 12 V Diachroic, Philips 50Par30L-WFL40, Osram 12 V

Diachroic, Concord 2627632 MK41, DAL Baltic 64005, Sylvania TrueAim-Titan MR16, Erco Eclipse-Clear Lens, Philips Philips 50 W MR16, GE EYC 71 W MR16, GE Par38 (11878), Luxina EXZ-CG-M250 MR16, GE Par 38 80 W Flood, Osram Par 38 120 W, GE Par 38 80 W Spot, and GE Standard Tungsten) were selected [21]. The root mean square error (RMSE) and goodness of fit coefficient (GFC) were employed to evaluate the spectral difference between the original and reconstructed testing samples [22]. The smaller the RMSE the closer the original spectrum, while the GFC is just the reverse.

4. Results and Discussion

The performance and feasibility of wLabPQR ICSs were tested by odd and even chips of Munsell as training and testing samples, respectively, comparing the results with the nonweighted LabPQR. The CIELAB color differences between the original and reconstructed spectrum of Munsell testing samples were calculated under various illuminants and light sources. The statistical results are shown in Table 1. It illustrated that wLabPQR ICSs results outperform non-weighted LabPQR ICS and ICS_WF3 performs best according to the experimental result. The mean color difference, the maximum color difference, and the percentage of testing samples with color differences greater than 3 of ICS_WF1 and ICS_WF2 are not much numerical difference, but these are a much smaller than that of ICS_NW. It indicated that the ICS_NW has obviously illuminant selective phenomenon. The last row of Table 1 shows the variance of the color difference statistics under all the illuminants and light sources of the four ICSs. The variances could represent the robustness of the four ICSs: the smaller the variance, the more robust the performance of the ICS under various illuminants and light sources [8]. The variance results indicate that ICS_WF3 is with the highest robustness and then are ICS_WF2 and ICS_WF1. The LabPQR is with relatively low robustness.

The RMSE and GFC statistics between the original and reconstructed reflectance of Munsell testing samples are shown in Table 2. It is shown that ICS_NW performed best and next is ICS_WF2 and ICS_WF3; the ICS_WF1 performs worst according to the experiment result. Similar results were shown by Laamanen et al. [17]: weighting clearly improves the reproduction of color information, but at the cost of the reproduction of spectral reflectance curve. The reason is that the higher the weight function numerical value, the lower the spectral reproduction error.

Figure 2 shows an example of spectral reconstructions of one Munsell spectrum formed with four ICSs. From the results it can be concluded that the middle part of the weighted spectrum is reconstructed more accurately than the nonweighted spectrum, but both ends of the spectrum are quite the contrary. The reason can be found from the curve shape of the weight function shown in Figure 1.

To access the medium dependence of the ICS, the colorimetric and spectral representing accuracy of the four ICSs were also evaluated with spectral image as testing samples. All the spectral reflectance of spectral image was transformed into the four ICSs and then transformed back to spectral reflectance with the Munsell chips as training

TABLE 1: Colorimetric representing accuracy comparison of the four ICSs with odd and even chips of Munsell as training and testing sample, respectively.

Illuminants	ΔE_{ab}												
	ICS_NW			ICS_WF1			ICS_WF2			ICS_WF3			
	Mean ^a	Max ^b	% >3 ^c	Mean	Max	% >3	Mean	Max	% >3	Mean	Max	% >3	
LED	Sylvania Concord 2048794	0.320	4.903	0.316	0.260	2.154	0.000	0.204	3.170	0.158	0.156	1.810	0.000
	Photon Star CS5	0.289	4.640	0.316	0.228	1.973	0.000	0.190	2.976	0.000	0.142	1.677	0.000
	Erco Optec Spotlights	0.316	4.052	0.316	0.252	2.146	0.000	0.245	2.277	0.000	0.243	1.917	0.000
	Synergy 1003605 S12	0.395	3.223	0.158	0.283	2.497	0.000	0.273	2.978	0.000	0.245	2.486	0.000
	Synergy 1003607 NF34	0.310	4.881	0.316	0.245	2.102	0.000	0.192	3.113	0.158	0.144	1.640	0.000
	Cooper DL11-WS-WW	0.336	3.280	0.158	0.264	2.251	0.000	0.228	2.825	0.000	0.193	2.000	0.000
	GE Par 30	0.311	3.269	0.158	0.257	2.275	0.000	0.220	2.262	0.000	0.205	1.705	0.000
	Philips EnduraLED MR16	0.327	3.743	0.316	0.264	2.034	0.000	0.231	2.608	0.000	0.222	2.016	0.000
	Erco Light Board V01	0.278	3.371	0.316	0.244	2.031	0.000	0.198	2.222	0.000	0.187	1.681	0.000
	MSI iPAR3830021D	0.333	4.122	0.316	0.265	2.491	0.000	0.243	2.145	0.000	0.225	2.109	0.000
	Erco ERCO Large Flood	0.279	3.434	0.316	0.249	1.903	0.000	0.197	2.328	0.000	0.184	1.465	0.000
	Philips Philips Par38	0.391	4.900	0.473	0.272	2.556	0.000	0.275	2.906	0.000	0.234	2.212	0.000
	Solais LR38	0.423	5.552	0.473	0.271	2.535	0.000	0.305	3.041	0.158	0.255	2.294	0.000
	Philips MASTER LEDspot MV	0.433	5.499	0.473	0.305	2.812	0.000	0.336	3.203	0.158	0.301	2.659	0.000
	TH	Solux 12 V Diachroic	0.127	1.979	0.000	0.060	0.675	0.000	0.068	1.070	0.000	0.040	0.317
Philips 50Par30L-WFL40		0.189	3.240	0.158	0.179	2.064	0.000	0.094	1.615	0.000	0.073	0.669	0.000
Osram 12 V Diachroic		0.266	4.539	0.316	0.222	2.446	0.000	0.143	2.346	0.000	0.096	0.965	0.000
Concord 2627632 MK41		0.269	4.565	0.316	0.248	2.732	0.000	0.139	2.252	0.000	0.106	1.037	0.000
DAL Baltic 64005		0.312	5.271	0.316	0.239	2.567	0.000	0.166	2.677	0.000	0.106	1.024	0.000
Sylvania TrueAim-Titan MR16		0.280	4.749	0.316	0.242	2.644	0.000	0.147	2.378	0.000	0.105	1.039	0.000
Erco Eclipse-Clear Lens		0.301	5.159	0.316	0.280	3.041	0.158	0.151	2.502	0.000	0.119	1.177	0.000
Philips Philips 50 W MR16		0.316	5.277	0.316	0.269	2.903	0.000	0.168	2.650	0.000	0.118	1.182	0.000
GE EYC 71 W MR16		0.314	5.407	0.316	0.293	3.137	0.158	0.162	2.639	0.000	0.126	1.224	0.000
GE Par38 (11878)		0.334	5.715	0.316	0.304	3.265	0.158	0.173	2.795	0.000	0.130	1.268	0.000
Luxina EXZ-CG-M250 MR16		0.269	4.135	0.316	0.242	2.578	0.000	0.158	2.141	0.000	0.120	1.264	0.000
GE Par 38 80 W Flood		0.332	5.676	0.316	0.303	3.242	0.158	0.173	2.781	0.000	0.130	1.271	0.000
Osram Par 38 120 W		0.335	5.756	0.316	0.305	3.269	0.158	0.172	2.820	0.000	0.129	1.252	0.000
GE Par 38 80 W Spot		0.335	5.739	0.316	0.306	3.270	0.158	0.174	2.809	0.000	0.131	1.274	0.000
GE Standard Tungsten		0.397	6.835	0.631	0.365	3.703	0.158	0.219	3.384	0.158	0.163	1.664	0.000
CIE	A	0.282	4.900	0.316	0.255	2.849	0.000	0.137	2.385	0.000	0.104	0.976	0.000
	B	0.108	1.837	0.000	0.081	1.012	0.000	0.050	0.875	0.000	0.039	0.246	0.000
	C	0.100	1.411	0.000	0.062	0.670	0.000	0.080	0.913	0.000	0.066	0.687	0.000
	D50	0.071	0.954	0.000	0.087	0.966	0.000	0.051	0.661	0.000	0.050	0.596	0.000
	D55	0.042	0.528	0.000	0.053	0.590	0.000	0.031	0.392	0.000	0.030	0.365	0.000
	D75	0.027	0.304	0.000	0.038	0.427	0.000	0.022	0.263	0.000	0.022	0.266	0.000
Statistic	Mean	0.279	4.081	0.266	0.231	2.280	0.032	0.172	2.297	0.023	0.141	1.355	0.000
	Maximum	0.433	6.835	0.631	0.365	3.703	0.158	0.336	3.384	0.158	0.301	2.659	0.000
	Variance	0.011	2.623	0.023	0.007	0.712	0.004	0.006	0.692	0.003	0.005	0.404	0.000

^aMean means the mean value of testing samples with color differences.

^bMax means the maximal value of testing samples with color differences.

^c% >3 means the percentage of testing samples with color differences greater than 3 CIELAB units.

TABLE 2: Spectral representing accuracy comparison of the four ICSs with odd and even chips of Munsell as training and testing samples, respectively.

	ICS_NW			ICS_WF1			ICS_WF2			ICS_WF3		
	Min.	Mean	Max.	Min.	Mean	Max.	Min.	Mean	Max.	Min.	Mean	Max.
RMSE	0.0011	0.0080	0.0528	0.0016	0.0148	0.0894	0.0012	0.0091	0.0604	0.0012	0.0115	0.0800
GFC	0.9387	0.9990	1.0000	0.8644	0.9968	1.0000	0.9272	0.9988	1.0000	0.8940	0.9981	1.0000

TABLE 3: Colorimetric representing accuracy comparison of the four ICSs with chips of Munsell and spectral image as training and testing sample, respectively.

Illuminants	ΔE_{ab}												
	ICS_NW			ICS_WF1			ICS_WF2			ICS_WF3			
	Mean	Max	% >3	Mean	Max	% >3	Mean	Max	% >3	Mean	Max	% >3	
LED	Sylvania Concord 2048794	1.205	6.520	4.917	0.691	3.478	0.037	0.644	5.142	0.797	0.386	2.421	0.000
	Photon Star CS5	1.061	5.325	3.104	0.666	3.170	0.016	0.588	3.918	0.219	0.396	1.884	0.000
	Erco Optec Spotlights	0.795	6.620	2.313	0.709	3.398	0.026	0.581	4.237	0.370	0.615	2.768	0.000
	Synergy 1003605 S12	1.227	7.054	4.438	0.640	3.122	0.005	0.729	6.949	1.828	0.479	3.992	0.229
	Synergy 1003607 NF34	1.087	5.671	2.479	0.672	3.405	0.021	0.634	5.712	0.865	0.468	3.349	0.037
	Cooper DL11-WS-WW	1.117	7.045	2.552	0.652	3.496	0.026	0.641	6.356	1.354	0.415	3.316	0.026
	GE Par 30	0.863	4.661	0.734	0.644	3.346	0.010	0.477	4.277	0.167	0.402	2.428	0.000
	Philips EnduraLED MR16	0.992	4.964	1.875	0.664	3.396	0.016	0.576	4.356	0.255	0.473	2.617	0.000
	Erco Light Board V01	0.829	4.027	0.578	0.658	3.189	0.010	0.495	2.864	0.000	0.462	2.208	0.000
	MSI iPAR3830021D	0.802	5.847	1.906	0.712	3.529	0.063	0.487	3.509	0.089	0.506	2.391	0.000
	Erco ERCO Large Flood	0.888	3.985	0.797	0.663	3.259	0.021	0.514	3.087	0.010	0.442	2.126	0.000
	Philips Philips Par38	1.055	6.410	3.276	0.721	3.539	0.063	0.599	4.000	0.380	0.529	2.471	0.000
	Solais LR38	1.117	7.657	3.875	0.704	3.367	0.037	0.654	4.810	1.188	0.572	2.423	0.000
	Philips MASTER LEDspot MV	1.131	8.575	4.370	0.794	3.867	0.125	0.783	5.667	1.865	0.751	3.297	0.031
	TH	Solux 12 V Diachroic	0.448	2.420	0.000	0.153	0.731	0.000	0.200	1.415	0.000	0.066	0.332
Philips 50Par30L-WFL40		0.695	3.654	0.042	0.457	2.300	0.000	0.239	2.122	0.000	0.158	0.680	0.000
Osram 12 V Diachroic		0.981	4.876	2.474	0.547	2.764	0.000	0.374	2.839	0.000	0.190	1.042	0.000
Concord 2627632 MK41		0.987	5.005	2.406	0.615	3.078	0.005	0.354	2.839	0.000	0.228	1.083	0.000
DAL Baltic 64005		1.139	5.648	5.646	0.567	2.800	0.000	0.441	3.191	0.005	0.182	1.132	0.000
Sylvania TrueAim-Titan MR16		1.031	5.158	3.323	0.593	2.958	0.000	0.383	2.931	0.000	0.212	1.135	0.000
Erco Eclipse-Clear Lens		1.116	5.581	4.760	0.692	3.412	0.026	0.400	3.110	0.005	0.262	1.236	0.000
Philips Philips 50 W MR16		1.154	5.758	5.531	0.651	3.259	0.005	0.435	3.279	0.010	0.238	1.353	0.000
GE EYC 71 W MR16		1.162	5.821	5.719	0.710	3.537	0.042	0.418	3.247	0.005	0.271	1.321	0.000
GE Par38 (11878)		1.231	6.099	7.115	0.737	3.699	0.063	0.444	3.407	0.037	0.283	1.369	0.000
Luxina EXZ-CG-M250 MR16		0.962	4.856	1.943	0.576	2.852	0.000	0.380	2.906	0.000	0.226	1.500	0.000
GE Par 38 80 W Flood		1.222	6.061	6.964	0.737	3.686	0.063	0.443	3.391	0.037	0.283	1.369	0.000
Osram Par 38 120 W		1.234	6.122	7.250	0.743	3.727	0.068	0.445	3.426	0.042	0.283	1.338	0.000
GE Par 38 80 W Spot		1.234	6.113	7.177	0.744	3.724	0.068	0.446	3.417	0.037	0.286	1.368	0.000
GE Standard Tungsten		1.484	7.053	11.219	0.861	4.265	0.375	0.568	3.913	0.344	0.350	1.838	0.000
CIE	A	1.041	5.261	3.609	0.635	3.197	0.005	0.362	2.947	0.000	0.230	1.001	0.000
	B	0.372	2.244	0.000	0.248	1.087	0.000	0.146	1.258	0.000	0.107	0.483	0.000
	C	0.266	2.047	0.000	0.107	0.534	0.000	0.169	1.371	0.000	0.116	0.774	0.000
	D50	0.259	1.378	0.000	0.213	1.032	0.000	0.114	0.942	0.000	0.109	0.601	0.000
	D55	0.150	0.793	0.000	0.130	0.632	0.000	0.067	0.548	0.000	0.067	0.363	0.000
	D75	0.093	0.474	0.000	0.095	0.459	0.000	0.045	0.342	0.000	0.049	0.258	0.000
Statistic	Mean	0.927	5.051	3.211	0.583	2.894	0.034	0.436	3.363	0.283	0.317	1.693	0.009
	Maximum	1.484	8.575	11.219	0.861	4.265	0.375	0.783	6.949	1.865	0.751	3.992	0.229
	Variance	0.120	3.698	7.375	0.044	1.115	0.004	0.034	2.345	0.270	0.029	0.926	0.002

TABLE 4: Spectral representing accuracy comparison of the four ICSs with chips of Munsell and spectral image as training and testing sample, respectively.

	ICS_NW			ICS_WF1			ICS_WF2			ICS_WF3		
	Min.	Mean	Max.	Min.	Mean	Max.	Min.	Mean	Max.	Min.	Mean	Max.
RMSE	0.0024	0.0117	0.0634	0.0032	0.0194	0.0894	0.0025	0.0131	0.0659	0.0030	0.0162	0.0792
GFC	0.9182	0.9866	1.0000	0.7618	0.9645	0.9999	0.8910	0.9825	1.0000	0.8308	0.9743	1.0000

TABLE 5: Overall performance of the four ICSs.

ICS	Dimension	Spectral accuracy	Colorimetric accuracy	Robustness
ICS_NW	6	Highest	Low	Low
ICS_WF1	6	Low	Higher	Higher
ICS_WF2	6	Higher	High	High
ICS_WF3	6	High	Highest	Highest

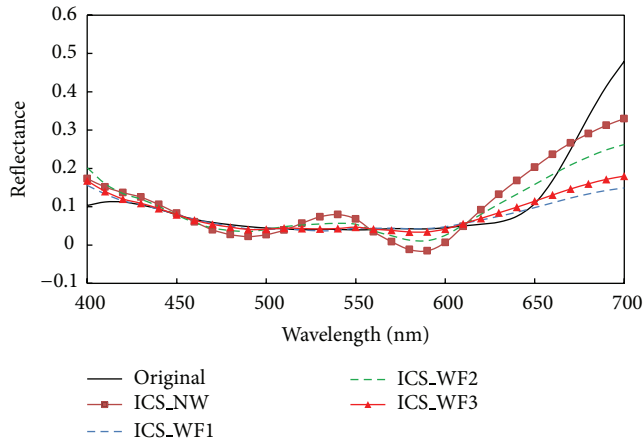


FIGURE 2: Example of the spectral reconstructions of one Munsell spectrum.

samples. The statistics of color and spectral difference under all the illuminants and light sources between the original and reconstructed spectrum are illustrated in Tables 3 and 4, respectively. It indicated that the colorimetric and the spectral representing accuracy of spectral image are lower than Munsell testing samples as a whole for all four ICSs. As results presented, the comparative results in the spectral and colorimetric representing accuracy of the four ICSs for the spectral image have similar trends with the Munsell testing samples. The wLabPQR clearly improved the color reproduction accuracy comparing to the nonweighted LabPQR, even though it decreased slightly the spectral reproduction accuracy. In addition, the robust performance of the ICS_WF1 is relatively higher than that of ICS_WF2 under various illuminants and light sources.

The overall performances of the four ICSs are shown Table 5. It illustrated that the performance orders of the four ICSs are ICS_WF3, ICS_WF1, ICS_WF2, and ICS_NW according to the experimental results. The ICS_NW is with high spectral but low colorimetric representing accuracy and robustness, and it is not suitable for spectral color reproduction, while the wLabPQR is with low spectral but high colorimetric representing accuracy and robustness; ICS_WF3 is especially most suitable for spectral color reproduction at low dimension.

5. Conclusion

In this paper, the weighted LabPQR method was presented for spectral color reproduction. The method is largely based

on nonweighted LabPQR, but it differs from the normal LabPQR in that PQR dimensions of LabPQR are weighted by the human color vision. This is done to retain more color information rather than spectral information in spectral color reproduction.

To evaluate the performance and feasibility of the weighed LabPQR, PQR dimensions are weighted by three different weight functions based on human color vision composed of the three ICSs (ICS_WF1, ICS_WF2, and ICS_WF3). The reflectance of the color chips of Munsell and spectral image was employed as the samples in this study. As results presented, weighting obviously improves the colorimetric representing accuracy and robustness, but at the cost of the spectral representing accuracy. However, the weighted LabPQR ICSs achieve more accurate reconstruction at higher human eye sensitive wavelengths that retain an amount of human color vision information. These results further imply that weight function WF3 proposed in this study outperformed the other two weight functions, and ICS_WF3 is most suitable for spectral color reproduction.

Conflict of Interests

The authors declare that there is no conflict of interests regarding the publication of this paper.


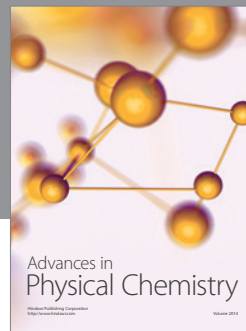
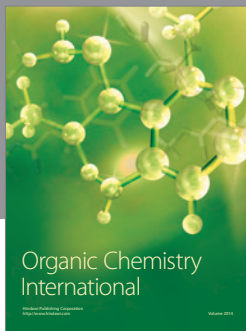
Acknowledgments

This study was supported by the National Natural Science Foundation of China (no. 41271446) and the Innovation Fund Project for Graduate Student of Shanghai (no. JWCXSL1401).

References

- [1] H.-L. Shen and J. H. Xin, "Estimation of spectral reflectance of object surfaces with the consideration of perceptual color space," *Optics Letters*, vol. 32, no. 1, pp. 96–98, 2007.
- [2] B. Sun, H. Liu, and S. Zhou, "Spectral separation for multi-spectral image reproduction based on constrained optimization method," *Journal of Spectroscopy*, vol. 2014, Article ID 345193, 8 pages, 2014.
- [3] X. Zhang, Q. Wang, Y. Wang, and H. Wu, "XYZLMS interim connection space for spectral image compression and reproduction," *Optics Letters*, vol. 37, no. 24, pp. 5097–5099, 2012.
- [4] J. Mohtasham, A. S. Nateri, and H. Khalili, "Textile colour matching using linear and exponential weighted principal component analysis," *Coloration Technology*, vol. 128, no. 3, pp. 199–203, 2012.
- [5] E. M. Valero, Y. Hu, J. Hernández-Andrés et al., "Comparative performance analysis of spectral estimation algorithms and

- computational optimization of a multispectral imaging system for print inspection,” *Color Research and Application*, vol. 39, no. 1, pp. 16–27, 2014.
- [6] H. Haneishi, T. Hasegawa, A. Hosoi, Y. Yokoyama, N. Tsumura, and Y. Miyake, “System design for accurately estimating the spectral reflectance of art paintings,” *Applied Optics*, vol. 39, no. 35, pp. 6621–6632, 2000.
- [7] A. M. Bakke, I. Farup, and J.-Y. Hardeberg, “Multispectral gamut mapping and visualization- a first attempt,” in *Color Imaging X: Processing, Hardcopy, and Applications*, vol. 5667 of *Proceedings of SPIE*, pp. 193–200, Bellingham, Wash, USA, January 2005.
- [8] X. Zhang, Q. Wang, J. Li, P. Yang, and J. Yu, “The interim connection space based on human color vision for spectral color reproduction,” *Journal of the Optical Society of America A*, vol. 29, no. 6, pp. 1027–1034, 2012.
- [9] M. W. Derhak and M. R. Rosen, “Spectral colorimetry using LabPQR: an interim connection space,” *Journal of Imaging Science and Technology*, vol. 50, no. 1, pp. 53–63, 2006.
- [10] F. Nakaya and N. Ohta, “Spectral encoding/decoding using LabRGB,” *Journal of Imaging Science and Technology*, vol. 52, no. 4, 2008.
- [11] S. Tsutsumi, M. R. Rosen, and R. S. Berns, “Spectral gamut mapping using LabPQR,” *Journal of Imaging Science and Technology*, vol. 51, no. 6, pp. 473–485, 2007.
- [12] S. Tsutsumi, M. R. Rosen, and R. S. Berns, “Spectral color reproduction using an interim connection space-based lookup table,” *Journal of Imaging Science and Technology*, vol. 52, no. 4, pp. 04021-1–04021-13, 2008.
- [13] S. Tsutsumi, M. R. Rosen, and R. S. Berns, “Spectral color management using interim connection spaces based on spectral decomposition,” *Color Research and Application*, vol. 33, no. 4, pp. 282–299, 2008.
- [14] D.-Y. Tzeng and R. S. Berns, “A review of principal component analysis and its applications to color technology,” *Color Research and Application*, vol. 30, no. 2, pp. 84–98, 2005.
- [15] M. Flinkman, H. Laamanen, J. Tuomela, P. Vahimaa, and M. Hauta-Kasari, “Eigenvectors of optimal color spectra,” *Journal of the Optical Society of America A*, vol. 30, no. 9, pp. 1806–1813, 2013.
- [16] J. Tian and Y. Tang, “Wavelength-sensitive-function controlled reflectance reconstruction,” *Optics Letters*, vol. 38, no. 15, pp. 2818–2820, 2013.
- [17] H. Laamanen, T. Jetsu, T. Jaaskelainen, and J. Parkkinen, “Weighted compression of spectral color information,” *Journal of the Optical Society of America A*, vol. 25, no. 6, pp. 1383–1388, 2008.
- [18] F. Agahian, S. A. Amirshahi, and S. H. Amirshahi, “Reconstruction of reflectance spectra using weighted principal component analysis,” *Color Research & Application*, vol. 33, no. 5, pp. 360–371, 2008.
- [19] “Spectral Database, University of Eastern Finland Color Group,” <http://www.uef.fi/fi/spectral/spectral-database>.
- [20] H. J. Trussell and M. S. Kulkarni, “Sampling and processing of color signals,” *IEEE Transactions on Image Processing*, vol. 5, no. 4, pp. 677–681, 1996.
- [21] “Spectral power distribution (SPD) curves,” <http://research.ng-london.org.uk/scientific/spd/>.
- [22] F. H. Imai, M. R. Rosen, and R. S. Berns, “Comparative study of metrics for spectral match quality,” in *Proceedings of the 1st European Conference on Colour in Graphics, Imaging and Vision (CGIV '02)*, pp. 492–496, Poitiers, France, April 2002.



Hindawi

Submit your manuscripts at
<http://www.hindawi.com>

